

Vessel Wall Models for Simulation of Atherosclerotic Vascular Networks

Yu. Vassilevski¹¹, S. Simakov², V. Salamatova³, Yu. Ivanov³ and T. Dobroserdova⁴

¹ Institute of Numerical Mathematics RAS,
Gubkina st. 8, Moscow 119333, Russia

² Moscow Institute of Physics and Technology,
Institutskiy Lane 9, Dolgoprudny 141700, Russia

³ Scientific Educational Center of Institute of Numerical Mathematics RAS,
Gubkina st. 8, Moscow 119333, Russia

⁴ Lomonosov Moscow State University,
Leninskie Gory, Moscow 119991, Russia

Abstract. Two mathematical models of elastic walls of healthy and atherosclerotic blood vessels are developed and studied. The models are included in numerical model of global blood circulation via recovery of the vessel wall state equation. The joint model allows us to study the impact of atherosclerotic arteries on regional haemodynamics.

Key words: atherosclerosis, mathematical modelling, blood flow, arterial wall, wall state equation
AMS subject classification: 35Q92, 76Z05, 65M06, 65M25

1. Introduction

Vascular diseases are the main factors of mortality, and atherosclerosis is the most common vascular disease. Advanced medical treatment of atherosclerosis is one of the challenges for contemporary medicine. A study of vascular diseases and, in particular, of atherosclerosis impact on haemodynamics may be based on mathematical models and numerical simulation [2, 7, 11, 14, 16, 17]. It is supposed to use the closed blood circulation model [14] in which the elastic properties of blood

¹Corresponding author. E-mail: vasilevs@dodo.inm.ras.ru

vessels are included in the wall state equation. The latter sets up the dependence of lumen cross section on the transmural pressure. Vessel diseases impact may be incorporated into the model through the recovery of the diseased vessel state equation. We suggest to derive the diseased wall state equation on the basis of the numerical solution of the equilibrium problem for simplified elastic fiber-spring system which imitates the atherosclerotic vessel reaction to deformation. The fiber-spring model was introduced in [17] where all materials were considered as linear.

In this paper we introduce approaches to modelling of atherosclerotic vessels elastic properties as nonlinear material ones. The key relationship in the theory of elasticity is the stress-strain relationship. Most bio-materials are nonlinear [4], arterial walls being the representative example. To review constitutive equations for arterial material we refer to [5, 6, 18]. We have applied a Neo-Hookean solid model which was used in modelling of atherosclerotic vessels [9] and aneurysms development study [19].

Two models of nonlinear elasticity for healthy and diseased vessels were developed. The first model is analytical and restricted by simple geometries of the vessel and the plaque. The second model is numerical and applies to much wider class of plaque geometry. We validate our numerical model via the analytical model and reproduce the state equation of the diseased wall. The recovered wall state equation allows us to employ the haemodynamic model and predict atherosclerotic plaques impact on the blood flow regime.

The outline of the paper is following. In Section 2 analytical thin-walled and numerical fiber models of healthy artery are considered. Analytical three-layer and numerical fiber-spring models of atherosclerotic artery are presented in Section 3. Section 4 deals with the network blood flow model. In Section 5 the numerical results are presented. Section 6 sums up the paper.

2. Elasticity models of healthy vessel

This section presents two elastic models for a healthy vessel wall considered as Neo-Hookean material. The first model is based on analytic solution of equilibrium problem for the thin-walled cylinder composed of Neo-Hookean material. Applicability of this approach is limited by vessels with straight cylindrical geometry. The second model uses a fiber representation of a vessel elastic wall. It benefits a simple finite difference discretization scheme and applicability to general geometries of blood vessels. In Section 5 we validate the fiber model via the reference solution obtained by the thin-wall model. The fiber model of a healthy vessel forms the basis for more complex atherosclerotic vessel model than presented in Section 3.

2.1. Thin-wall model

We consider a blood vessel as a thin-walled circular cylindrical shell inflated by the internal pressure. A strain in the axial direction is assumed to be negligible. The mechanical behavior of the arterial wall is defined by the incompressible Neo-Hookean material model. The Neo-Hookean

solid is characterized by a strain energy density function W which for the incompressible case is

$$W = \frac{\mu}{2}(\lambda_1^2 + \lambda_2^2 + \lambda_3^2 - 3), \quad (2.1)$$

where μ is the material constant, λ_i are the principal stretches. For the incompressible Neo-Hookean material the relationship between the initial Young's modulus of the vessel (arterial) wall and the material constant μ is the following $\mu = E/3$. The principal components of the Cauchy stress for the incompressible hyperelastic material are given by

$$\sigma_i = -p + \lambda_i \frac{\partial W}{\partial \lambda_i}, \quad i = 1, 2, 3, \quad (2.2)$$

where p is pressure to be determined.

In terms of the cylindrical polar coordinates (R, Θ, Z) the geometry of the tube is defined by $R_0 - H/2 \leq R \leq R_0 + H/2$, where R_0 and H denote the middle radius and the thickness of the non-deformed tube, respectively.

The tube middle radius and thickness with respect to the axisymmetric deformed configuration are denoted by r_0 and h , respectively. In terms of cylindrical polar coordinates (r, θ, z) the tube under internal pressure p_0 is given by $r_0 - h/2 \leq r \leq r_0 + h/2$.

In our case the principal stretches are stretches in radial, circumferential and axial directions, i.e., λ_r , λ_θ and λ_z , respectively. They are defined by

$$\lambda_r = h/H, \quad \lambda_\theta = r_0/R_0, \quad (2.3)$$

and $\lambda_z = 1$ due to the assumption that the strain in the axial direction is negligible. Thus the incompressibility constraint is

$$\lambda_r \lambda_\theta \lambda_z = \lambda_r \lambda_\theta = 1. \quad (2.4)$$

Using the simplification $\sigma_r = -p + \lambda_r \partial W / \partial \lambda_r = 0$ for the radial stress (the membrane approximation) we can find the pressure $p = \lambda_r \partial W / \partial \lambda_r = \mu \lambda_r^2$. The circumferential stress σ_θ is assumed to be approximately constant through the tube thickness; then balancing the tension in the tube and the inflation pressure we find that

$$p_0 = \frac{h \sigma_\theta}{r_i}, \quad (2.5)$$

where $r_i = r_0 - h/2$ is internal radius of the deformed cylinder and

$$\sigma_\theta = \mu(\lambda_\theta^2 - \lambda_r^2). \quad (2.6)$$

Taking into account (2.3), (2.4) and (2.5) we can write the following system of equations in two unknowns λ_θ and λ_r

$$\begin{cases} \lambda_r \lambda_\theta = 1, \\ \mu(\lambda_\theta^2 - \lambda_r^2) = \frac{p_0}{\lambda_r H} \left(\lambda_\theta R_0 - \frac{\lambda_r H}{2} \right). \end{cases} \quad (2.7)$$

System (2.7) reduces to a bi-quadratic equation on λ_θ (or λ_r) and thus may be solved analytically. Knowing solution of the system (2.7) we can find circumferential stress σ_θ , the pressure p and the geometrical parameters of the deformed tube h and R .

2.2. Fiber model

Using the approach described in [13], we imitate a response of the elastic surface to a deformation as the response of fibers collection to the same deformation. Let $\vec{X}(s, t)$ represent the fiber points position in space, where Lagrange coordinate s is an arc length of the fiber in the unstressed state. We denote the fiber tension as $T(s, t)$. The local force density is given by the expression [15]:

$$\vec{f} = \frac{\partial}{\partial s}(T\vec{\tau}), \quad (2.8)$$

where $\vec{\tau}$ is the unit tangent vector

$$\vec{\tau} = \frac{\partial \vec{X}}{\partial s} \left| \frac{\partial \vec{X}}{\partial s} \right|^{-1}. \quad (2.9)$$

In case of axisymmetric problem we can assume the middle surface of the cylindrical shell as a collection of independent ring fibers, and the fiber tension is defined by (2.6), i.e.

$$T = \mu(\lambda_\theta^2 - \lambda_\theta^{-2}), \lambda_\theta = \left| \frac{\partial X}{\partial s} \right|. \quad (2.10)$$

Combining (2.8) with (2.10) results in final fiber-based stress-strain problem.

In case of Hookean wall material we use fiber tension in form [17]:

$$T = E_* \left(\left| \frac{\partial X}{\partial s} \right| - 1 \right), \quad (2.11)$$

where E_* is the elastic modulus of the fiber.

We derive the numerical approximation of the fiber model following [13, 15]. Let N_θ be the number of computational nodes on the fiber, \vec{X}_k be the coordinates of the k th node, $k = 1, \dots, N_\theta$, Δs be the distance between neighboring nodes along the non-deformed fiber. We assume that Δs will be the same for all fibers. In accordance with formulas (2.10), (2.11) we discretize T and $\vec{\tau}$:

$$T_{k+1/2} = \mu \left(\left(\frac{|\vec{X}_{k+1} - \vec{X}_k|}{\Delta s} \right)^2 - \left(\frac{|\vec{X}_{k+1} - \vec{X}_k|}{\Delta s} \right)^{-2} \right), \quad (2.12)$$

and in case of linear tension:

$$T_{k+1/2} = E_* \left(\frac{|\vec{X}_{k+1} - \vec{X}_k|}{\Delta s} - 1 \right), \quad (2.13)$$

$$\vec{\tau}_{k+1/2} = \frac{\vec{X}_{k+1} - \vec{X}_k}{|\vec{X}_{k+1} - \vec{X}_k|}. \quad (2.14)$$

The discrete elastic force at k th node is defined as

$$\vec{f}_k = \frac{T_{k+1/2}\vec{\tau}_{k+1/2} - T_{k-1/2}\vec{\tau}_{k-1/2}}{\Delta s}. \quad (2.15)$$

The above formulas set up our numerical fiber elastic model of the response to deformation.

3. Elasticity models of atherosclerotic vessel

Interior wall of an atherosclerotic vessel is covered by atherosclerotic plaques. Each plaque is composed of a thin fibrous cap and a lipid pool, and may cover lengthy parts of blood vessels. Mechanical studies show that besides the arterial wall, fibrous cap and lipid pool are composed by nonlinear materials as well.

Following the strategy of Section 2 we present two elastic models for an atherosclerotic vessel with a lengthy plaque. The first model represents the diseased vessel as a three-layer circular cylindrical shell inflated by internal pressure. The internal and external layers are thin-walled cylindrical shells which represent the plaque fibrous cap and the vessel wall, respectively (see Fig. 1). The middle layer represents the lipid pool of the plaque. In contrast to [17] we assume that the materials forming all three layers are incompressible Neo-Hookean solids. This model is limited to cylindrical vessels with uniform and lengthy plaques. In this case the deformation problem reduces to a system of nonlinear equations which can be solved semi-analytically. The solution provides geometric characteristics of the equilibrium state for any internal pressure, and, in particular, the dependence of a lumen cross section on the transmural pressure.

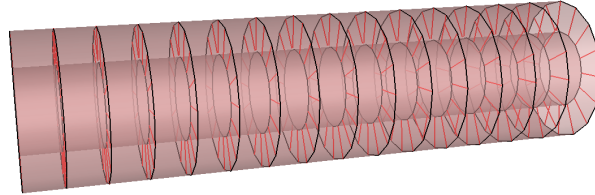


Figure 1: Geometry of the plaque.

The second model uses fiber representations of the arterial wall and the fibrous cap. The lipid pool is imitated by a set of radial springs with nonlinear relation between reaction force and displacement. An equilibrium state recovered by the above mentioned fiber-spring system is obtained in the framework of numerical approximation: finite difference discretization results in a system of nonlinear algebraic equations which has to be solved iteratively. This model benefits the wide class of plaque geometries. For instance, the Hookean materials fiber-spring model has been successfully tested for lengthy and local, symmetric and non-symmetric, plaques [17]. In Section 5 we validate the Non-Hookean materials fiber-spring model by solving the deformation problem for vessel with a lengthy atherosclerotic plaque using the first three-layer model.

3.1. Equilibrium of thick-walled cylinder

We consider a thick-walled cylinder under internal pressure p_a and external pressure p_b . The deformation is defined by the mapping

$$r = r(R), \quad \theta = \Theta, \quad z = Z. \quad (3.1)$$

Then the principal stretches in radial, circumferential and axial directions, λ_r , λ_θ and λ_z are

$$\lambda_r = \frac{dr}{dR}, \quad \lambda_\theta = \frac{r}{R}, \quad \lambda_z = \frac{dz}{dZ} = 1. \quad (3.2)$$

Using and integrating the incompressibility constraint $\lambda_r \lambda_\theta \lambda_z = 1$ we can obtain

$$r^2 = R^2 - K, \quad (3.3)$$

where K is the constant of integration.

It has been shown [3] that the equilibrium equation along radial direction is

$$R^2 \frac{dW}{dr} dr = K \frac{d\sigma_r}{dr}, \quad (3.4)$$

which after integration gives

$$p_a = p_b + \frac{1}{K} \int_{r_a}^{r_b} R^2 \frac{dW}{dr} dr, \quad (3.5)$$

where W is the stress energy density function defined by (2.1) for the cylinder and $W = W(r)$.

3.2. Three-layer circular cylindrical shell

The geometry of the non-deformed three-layer cylinder is defined by the following inequalities: $R_1 \leq R \leq R_2$ defines the fibrous cap, $R_2 < R \leq R_3$ defines the lipid pool, $R_3 < R \leq R_4$ defines the arterial wall. The deformation is represented by mapping (3.1) and $r_i = r(R_i)$, $i = 1, 2, 3, 4$. The three-layer cylinder is inflated by internal pressure p_0 .

Then we can write equations describing the deformation of each layer of the three-layer cylindrical tube: for the fibrous cap an equilibrium equation and an incompressibility constraint are expressed as

$$\begin{aligned} \mu_f((\lambda_\theta^f)^2 - (\lambda_r^f)^2) &= \frac{p_0 r_1 - p_1 r_2}{r_2 - r_1}, \\ \lambda_\theta^f \lambda_r^f &= 1; \end{aligned} \quad (3.6)$$

for the lipid pool an equilibrium equation is

$$p_1 = p_2 + \frac{1}{K} \int_{r_2}^{r_3} R^2 \frac{dW}{dr} dr; \quad (3.7)$$

for the arterial wall there is

$$\begin{aligned}\mu_a((\lambda_\theta^a)^2 - (\lambda_r^a)^2) &= \frac{p_2 r_3}{r_4 - r_3}, \\ \lambda_\theta^a \lambda_r^a &= 1,\end{aligned}\tag{3.8}$$

where p_1 and p_2 are contact pressures on surface $r = r_2$ and $r = r_3$, respectively; μ_f and μ_a are the material constants of the cap and the vessel wall, each of them being equal to corresponding initial Young's modulus divided by three ($\mu = E/3$); $\lambda_r^f, \lambda_\theta^f$ and $\lambda_r^a, \lambda_\theta^a$ are the principal stretches in radial and circumferential directions for the fibrous cap and the arterial wall, respectively; W is the strain energy density (2.1) which characterizes the lipid pool.

From continuity conditions of radial displacements and incompressibility constraints, we can find that

$$\begin{aligned}r^2 &= R^2 - K, \\ \lambda_\theta^f &= \frac{r_1 + r_2}{R_1 + R_2} = \frac{\sqrt{R_1^2 - K} + \sqrt{R_2^2 - K}}{R_1 + R_2}, \\ \lambda_\theta^a &= \frac{r_3 + r_4}{R_3 + R_4} = \frac{\sqrt{R_3^2 - K} + \sqrt{R_4^2 - K}}{R_3 + R_4}.\end{aligned}\tag{3.9}$$

Thus we can write system of equations describing the deformation of the three-layer cylindrical tube under internal pressure p_0 :

$$\begin{cases} \mu_f((\lambda_\theta^f)^2 - (\lambda_r^f)^2) = \frac{p_0 r_1 - p_1 r_2}{r_2 - r_1}, \\ p_1 = p_2 + \frac{1}{K} \int_{r_2}^{r_3} R^2 \frac{dW}{dr} dr, \\ \mu_a((\lambda_\theta^a)^2 - (\lambda_r^a)^2) = \frac{p_2 r_3}{r_4 - r_3}, \end{cases}\tag{3.10}$$

where $r(R), \lambda_\theta^f, \lambda_\theta^a$ are defined by (3.9) and the system (3.10) is the system of nonlinear equations with three unknowns p_1, p_2 , and K . The solution of this system defines each layer principal stretches and may be obtained by conventional software (e.g. MAPLE).

3.3. Fiber-spring model

We use the fiber model for the fibrous cap and the arterial wall. An elastic model of the lipid pool is based on its representation by a set of radial springs. In order to estimate spring displacement, we use a solution of the deformation problem for the incompressible isotropic cylinder ($a \leq r \leq b$) under internal pressure p_a and external pressure p_b . Since we work within the normal physiological range of blood pressure, we solve the deformation problem using the hypothesis of linear elasticity theory. In this case the relation between the radial displacement $u(r)$ of cylinder's points and given pressures is expressed as

$$p_a - p_b = \frac{2(b^2 - a^2)E_c r}{3a^2 b^2} u(r),\tag{3.11}$$

where E_c is Young's modulus of the cylinder.

For each radial spring, displacements of its end points are derived on the basis of (3.11) and the assumption that only radial displacements may occur. The unknown fields of fibrous cap and arterial wall radial displacements are specified by $u^a(\theta, z)$ and $u^b(\theta, z)$, respectively.

Balancing forces on the external (artery) and internal (fibrous cap) layers implies

$$p_a = p_0 - (\vec{f}^{\text{cap}}, \vec{n}^{\text{cap}})h^{\text{cap}}, \quad (3.12)$$

$$p_b = (\vec{f}^{\text{art}}, \vec{n}^{\text{art}})h^{\text{art}}, \quad (3.13)$$

where $\vec{f}^{\text{art}}, \vec{n}^{\text{art}}, h^{\text{art}}$ and $\vec{f}^{\text{cap}}, \vec{n}^{\text{cap}}, h^{\text{cap}}$ are force density, surface normal, layer thickness of the artery wall and the fibrous cap, respectively. Similarly to radial displacements $u^a(\theta, z), u^b(\theta, z)$, the forces, normals and thicknesses are functions of coordinates θ, z . Moreover, due to (2.8) and (2.4) these functions depend on radial displacements as well:

$$\vec{f}^{\text{cap}} = \vec{f}(a + u^a(\theta, z), \theta, z), \quad \vec{n}^{\text{cap}} = \vec{n}^{\text{cap}}(a + u^a(\theta, z), \theta, z), \quad h^{\text{cap}} = H^{\text{cap}}a/(a + u^a), \quad (3.14)$$

$$\vec{f}^{\text{art}} = \vec{f}(b + u^b(\theta, z), \theta, z), \quad \vec{n}^{\text{art}} = \vec{n}^{\text{art}}(b + u^b(\theta, z), \theta, z), \quad h^{\text{art}} = H^{\text{art}}b/(b + u^b), \quad (3.15)$$

where \vec{f} is given by (2.8), H^{cap} and H^{art} are thicknesses of fibrous cap and artery wall in non-stressed state.

In accordance with (3.12), (3.13) and (3.11) for $r = a$ and $r = b$, the radial displacements fields satisfy the following equations:

$$\begin{cases} (\vec{f}^{\text{art}}, \vec{n}^{\text{art}})h^{\text{art}} + (\vec{f}^{\text{cap}}, \vec{n}^{\text{cap}})h^{\text{cap}} - p_0 = u^a 2(b^2 - a^2)E_c/3ab^2, \\ (\vec{f}^{\text{art}}, \vec{n}^{\text{art}})h^{\text{art}} + (\vec{f}^{\text{cap}}, \vec{n}^{\text{cap}})h^{\text{cap}} - p_0 = u^b 2(b^2 - a^2)E_c/3a^2b. \end{cases} \quad (3.16)$$

The numerical model is based on equidistant N_z pairs of concentric ring fibers with coordinates $z_i, i = 1, \dots, N_z$, discretized by the same number of grid nodes with uniform angular distribution $\theta_k, k = 1, \dots, N_\theta$. The discretized system of equations (3.16) reads as

$$\begin{cases} (\vec{f}_{ik}^{\text{art}}, \vec{n}_{ik}^{\text{art}})h_{ik}^{\text{art}} + (\vec{f}_{ik}^{\text{cap}}, \vec{n}_{ik}^{\text{cap}})h_{ik}^{\text{cap}} - u_{ik}^a 2(b^2 - a^2)E_c a/3ab^2 = p_0, \\ (\vec{f}_{ik}^{\text{art}}, \vec{n}_{ik}^{\text{art}})h_{ik}^{\text{art}} + (\vec{f}_{ik}^{\text{cap}}, \vec{n}_{ik}^{\text{cap}})h_{ik}^{\text{cap}} - u_{ik}^b 2(b^2 - a^2)E_c b/3a^2b = p_0, \end{cases} \quad (3.17)$$

where

$$\begin{aligned} \vec{f}_{ik}^{\text{cap}} &= \vec{f}(a + u_{ik}^a, \theta_k, z_i), \\ \vec{f}_{ik}^{\text{art}} &= \vec{f}(b + u_{ik}^b, \theta_k, z_i), \\ \vec{n}_{ik}^{\text{cap}} &= \vec{n}(a + u_{ik}^a, \theta_k, z_i), \\ \vec{n}_{ik}^{\text{art}} &= \vec{n}(b + u_{ik}^b, \theta_k, z_i), \\ h_{ik}^{\text{cap}} &= \frac{H^{\text{cap}}a}{a + u_{ik}^a}, \\ h_{ik}^{\text{art}} &= \frac{H^{\text{art}}b}{b + u_{ik}^b}. \end{aligned}$$

The system of $2N_z N_\theta$ nonlinear equations (3.17) with $2N_z N_\theta$ unknowns u_{ik}^a, u_{ik}^b is solved by the Inexact Newton-Krylov method.

4. Network blood flow

We study atherosclerosis impact on the regional blood circulation using the closed circulation model [14]. In this section we briefly outline the model and discuss its functionality for vascular diseases simulation.

Blood flow is considered as a pulsating flow of incompressible fluid streaming through the network of elastic tubes (vessels). For every elastic tube (vessel) we account mass and momentum change by means of hyperbolic equations written in a characteristic form:

$$\partial S / \partial t + \partial(Su) / \partial x = 0, \quad (4.1)$$

$$\partial u / \partial t + \partial(u^2 / 2 + p / \rho) / \partial x = -16\mu u \eta(\hat{S}) / \hat{S}, \quad (4.2)$$

where t is a time, x is a coordinate along the vessel, ρ is a blood density, $S(t, x)$ is a vessel cross section area, $u(t, x)$ is linear flow velocity averaged over the vessel area at coordinate x , where p is pressure (with respect to the atmospheric pressure), function η is set as

$$\eta(\hat{S}) = \begin{cases} 2, & \hat{S} \geq 1, \\ \hat{S} + \frac{1}{\hat{S}}, & \hat{S} < 1. \end{cases} \quad (4.3)$$

Here $\hat{S} = S / \bar{S}$, \bar{S} is cross section area under zero transmural pressure $p(S) - p_*$ and zero velocity, p_* is a pressure in the surrounding tissues, μ is a friction factor.

The integration domain for (4.1), (4.2) is a set of 1D elastic tubes connected in a closed network according to the vascular anatomy. The structure of the systemic arterial network is shown in Fig. 2. The details for the methods of the closed vascular network 1D structure reconstruction and its parameters identification are given in [14]. The presented model is a global circulation model.

The vessels are connected with each other at the nodes and with the heart inlets/outlets through the boundary conditions set that is formed by Poiseuille's pressure drop conditions, mass balance equation combined with the appropriate compatibility condition for (4.1),(4.2):

$$p_k(S_k(t, \tilde{x}_k)) - p_{\text{node}}^l(t) = \varepsilon_k R_k^l S_k(t, \tilde{x}_k) u_k(t, \tilde{x}_k), \quad k = k_1, k_2, \dots, k_M, \quad (4.4)$$

$$\sum_{k=k_1, k_2, \dots, k_M} \varepsilon_k S_k(t, \tilde{x}_k) u_k(t, \tilde{x}_k) = 0, \quad (4.5)$$

where l is a node index, k is a vessel index, k_1, k_2, \dots, k_M and M are indexes and number of the vessels meeting at the node; $p_{\text{node}}^l(t)$ is a pressure at the vessels junction point; R_k^l is a hydraulic resistance for the flow from the k -th vessel to the l -th node. For the vessels incoming into a node we set $\varepsilon_k = 1, \tilde{x}_k = L_k$, for the outgoing vessels we set $\varepsilon_k = -1, \tilde{x}_k = 0$. At the heart junction

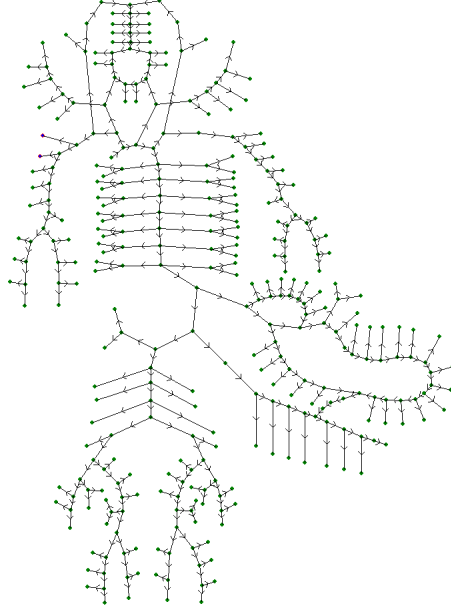


Figure 2: Systemic arterial network structure.

nodes the product $S_k(t, x) u_k(t, x)$ in (4.4), (4.5) is replaced by the volumetric flow to/from the chamber.

The vessel wall elastic properties are included in (4.1), (4.2) by the wall state equation giving the dependence of transmural pressure $p - p_*$ on the vessel cross section area S :

$$p(S) - p_* = \rho c_0^2 f(S), \quad (4.6)$$

where c_0 is the rate of small disturbance propagation in the vessel wall. For healthy vessels we use S -shaped function f [14]:

$$f(S) = \begin{cases} \exp(S/\bar{S} - 1) - 1, & S > \bar{S}, \\ \ln(S/\bar{S}), & S \leq \bar{S}, \end{cases} \quad (4.7)$$

which seems to be a feasible approximation of the experimental curves.

In general, function $f(S)$ depends on the type and state of the vessel wall and external factors: elastic or muscular type of the wall, installed endovascular devices, atherosclerotic plaque, occlusion, etc. It is difficult to estimate analytical approximation $f(S)$ for the above mentioned cases. In general, the wall state equation should be recovered in the mechanical laboratory study. We suggest to replace the expensive and time consuming experimental study with the vessel wall numerical models. The models apply to Hookean or Neo-Hookean elastic materials and provide discretized functional dependence (4.7). Similar approach with Hookean models have been developed in [16, 17].

For every vessel, the equations (4.1)-(4.7) are solved by the hybrid (first and second order) explicit grid-characteristic method. This model also includes a set of stiff ODEs which describes

the heart functioning in terms of volume averaged model [14]. The system of stiff ODEs is solved by A- and L-stable implicit third order Runge-Kutta method.

5. Results

Presentation of the numerical results have been divided into three parts.

In the first part we have studied our numerical fiber and fiber-spring models. Firstly, we have considered the healthy common carotid artery and validate the numerical fiber model via the analytical thin-walled model by comparing their wall state equations. Secondly, we analyze the lengthy atherosclerotic plaque on the common carotid artery with different lumens and validate the numerical fiber-spring model via the analytical three-layer model. These comparisons demonstrate acceptable errors of our numerical models and thus verify the presented approach.

In the second part we have studied the difference between Hookean and Neo-Hookean material models by comparing the discretized wall state equations for healthy and atherosclerotic artery.

The third part has demonstrated practical advantages of the developed elasticity models. These models are incorporated in the network blood flow model via the discretized wall state equations. We chose a region of the common carotid artery as an example of the atherosclerotic network.

5.1. Validation of fiber and fiber-spring models

Here we consider a straight cylindrical vessel and compare the analytical thin-wall model and the numerical fiber models. The wall material is assumed to be Neo-Hookean. The solution of the static equilibrium problem provides the dependence of cross sectional area S on the pressure load p_0 . Values of Young's modulus, an inner radius and a thickness of the arterial wall have been chosen according to the values known for the common carotid artery: $E = 10^6$ Pa [12], $R = 0.45$ cm and $H = 0.07$ cm, respectively. The computed pressure to relative cross section relationship is summarized in Table 1 where S_0 is an area of the healthy unloaded artery. We observe the error less than 1% for the whole range of pressures and less than 0.2% for pressures not exceeding 8 kPa. As we see later, the maximum blood pressure for the common carotid simulations is limited by this value.

Similarly we compare the solutions of the static equilibrium problem obtained by the analytical three-layer model and the numerical fiber-spring model of an atherosclerotic vessel. The lumen is set to 50%, 30% and 10%. The elastic constants and geometric characteristics correspond to the common carotid artery: Young's moduli for the arterial wall $E_{\text{art}} = 10^6$ Pa [12], the fibrous cap $E_{\text{cap}} = 5 \cdot 10^5$ Pa [8] and the lipid pool $E_{\text{pool}} = 10^3$ Pa [1], the thickness of the fibrous cap and the arterial wall $H_{\text{art}} = H_{\text{cap}} = 0.07$ cm. The computed pressure to relative cross section relationship is summarized in Table 2. We have obtained the error less than 2% in the whole range of pressures observed in the common carotid artery.

p_0 , kPa	S/S_0		error, %
	A	B	
0	1	0.9984	0.16
1	1.0113	1.0105	0.08
2	1.0230	1.0229	0.01
3	1.0350	1.0355	0.05
4	1.0475	1.0484	0.09
5	1.0604	1.0616	0.12
6	1.0737	1.0751	0.13
7	1.0875	1.0889	0.13
8	1.1018	1.1030	0.11
9	1.1166	1.1173	0.07
10	1.1320	1.1321	0.01
11	1.1480	1.1471	0.07
12	1.1646	1.1625	0.18
13	1.1819	1.1782	0.31
14	1.1999	1.1943	0.47

Table 1: Relative cross section of the common carotid artery under static pressure load p_0 obtained by analytical thin-walled model (A) and numerical fiber model (B).

5.2. Elasticity models for Hookean and Neo-Hookean materials

In [16, 17] we have used the Hookean (linear) material model in order to study the impact of elastic vessel properties changes due to the endovascular filter implantation or the atherosclerotic plaque occurrence. In this paper, we use the Neo-Hookean (nonlinear) material model for both healthy and atherosclerotic arteries. In this section we compare both material models in terms of the computed wall state equation in order to examine the difference between the two material models. Figure 3 demonstrates the dependencies $p_0(S/S_0)$ for the cases of healthy vessel (left panel) and atherosclerotic vessel with a lengthy plaque (right panel) and 10 % lumen. Parameters for the static equilibrium problem are set according to the common carotid artery properties.

In case of the healthy artery, we observe substantial deviation of the Hookean and Neo-Hookean curves $p_0(S/S_0)$ for pressures higher than 8 kPa. Since such high pressure is achieved no longer than 0.1 seconds within the cardiac cycle, the discrepancy impact on the wall state equations is almost negligible.

For the atherosclerotic artery, the discrepancy of the wall state equations is more distinct. The substantial pressures difference is observed for transmural pressures over 4 kPa as well as for negative transmural pressures. It results in higher sensitivity to inflating transmural pressure and higher resistivity to deflating transmural pressure.

p_0 , kPa	50% lumen			30% lumen			10% lumen		
	S/S_0		error,%	S/S_0		error,%	S/S_0		error,%
	A	B		A	B		A	B	
0	0.5000	0.4986	0.27	0.3000	0.2995	0.16	0.1000	0.0998	0.25
1	0.5044	0.5041	0.07	0.3028	0.3027	0.03	0.1008	0.1009	0.04
2	0.5089	0.5090	0.02	0.3056	0.3059	0.09	0.1016	0.1019	0.22
3	0.5134	0.5140	0.10	0.3085	0.3092	0.20	0.1025	0.1029	0.41
4	0.5181	0.5190	0.18	0.3115	0.3125	0.31	0.1034	0.1040	0.58
5	0.5228	0.5241	0.25	0.3145	0.3158	0.41	0.1042	0.1050	0.76
6	0.5277	0.5293	0.31	0.3176	0.3192	0.51	0.1051	0.1061	0.92
7	0.5326	0.5346	0.37	0.3208	0.3227	0.60	0.1060	0.1072	1.09
8	0.5376	0.5399	0.42	0.3240	0.3262	0.68	0.1070	0.1083	1.24
9	0.5428	0.5453	0.47	0.3273	0.3297	0.75	0.1079	0.1094	1.39
10	0.5480	0.5508	0.51	0.3306	0.3333	0.82	0.1089	0.1106	1.54
11	0.5534	0.5564	0.54	0.3341	0.3370	0.88	0.1099	0.1117	1.67
12	0.5589	0.5621	0.57	0.3376	0.3407	0.94	0.1109	0.1129	1.81
13	0.5645	0.5678	0.59	0.3411	0.3445	0.98	0.1119	0.1141	1.93

Table 2: Relative cross section of the atherosclerotic common carotid artery with lumen 50%, 30% and 10% under static pressure p_0 obtained by the analytical three-layer model (A) and numerical fiber-spring model (B).

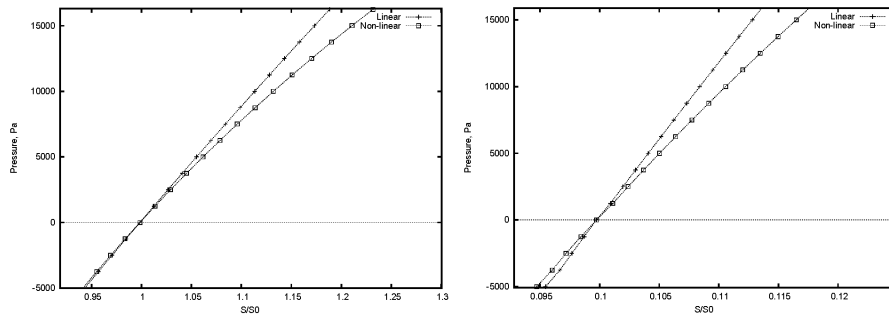


Figure 3: Comparison of wall state equations for Hookean and Neo-Hookean materials: healthy artery (left), atherosclerotic artery (right).

5.3. Blood flow in atherosclerotic vessels network

We have used the computed wall state equations (see Tables 1, 2) for atherosclerotic arteries in the network blood flow model. The following scenario of atherosclerosis has been chosen: the common, internal and external carotid arteries (vessels No. 9, 65, 66 in Fig. 4) are healthy or diseased with lengthy plaques and lumens are 50% or 30% whereas the other vessels are considered to be healthy. For the sake of brevity we consider a healthy vessel as an atherosclerotic vessel with 100% lumen. The wall state equation for vessels No. 9, 65, 66 is computed on the basis of the fiber-spring model for Neo-Hookean materials. The wall state equation for the other vessels is defined by analytical formulas (4.6), (4.7).

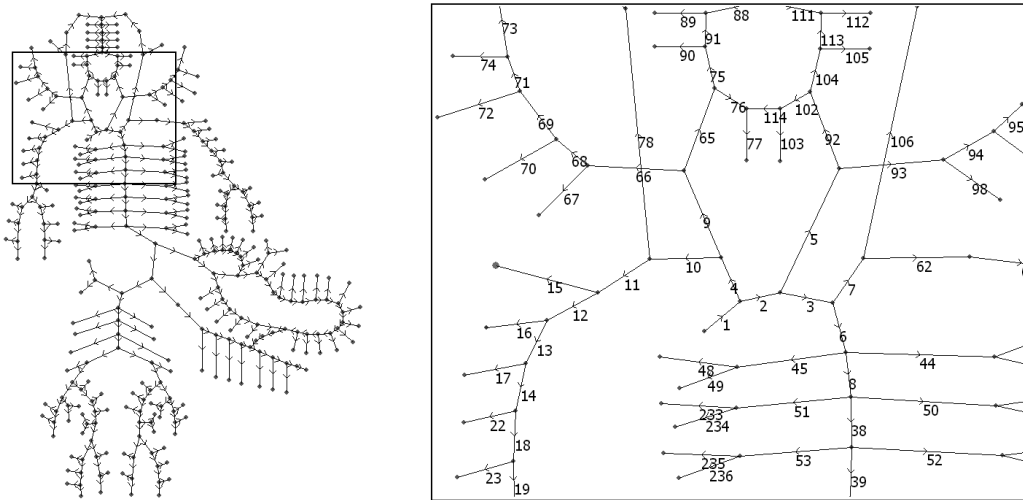


Figure 4: Fragment of the systemic arterial network.

In the first series of the experiments (see Figs. 5, 6, 7, 8) we assume that the right common carotid artery is damaged by the lengthy atherosclerotic plaque with 30%, 50% and 100% lumen. The pressure and velocity profiles in common (No. 9), subsequent internal (No. 65) and external (No. 66) carotid arteries are shown in Figs. 5, 6. The pressure and velocity profiles in the brachial artery (No. 12), external carotid continuation (No. 68) and the artery of the Willis circle (No. 91) are shown in Figs. 7, 8.

The left panel of Fig. 5 reveals no substantial changes of the pressure profile in the common carotid artery. The atherosclerosis affects only the velocity profile resulting in two-fold decrease of the maximum velocity under 30% lumen (see left panel of Fig. 6). This observation is confirmed by the well-known fact that haemodynamically noticeable atherosclerosis or stenosis has lumen less than 50%. The pressure and velocity profiles of the internal and external carotid arteries are affected much more noticeable (central and right panels of Figs. 5, 6). They reveal two-fold decrease of pressure and velocity maximums for the 30% lumen. The network blood flow model allows us to trace this effect throughout the entire network. For instance, considerable changes in

vessels No. 68 and No. 91 (see Figs. 7, 8) may be interpreted as initial stages of oxygen deficiency in such important parts as eye and brain. The pressure and velocity decrease in small vessels leads to thrombosis and subsequent sharp pressure increase. For the eye and the brain it results in ischemia, hemorrhage, blindness and stroke. These well known atherosclerosis consequences are also confirmed by the proposed mathematical model. The analysis of the collateral route (vessels No. 5, No. 92, No. 93 etc.) reveals no substantial changes in haemodynamics and is not presented here.

In the second series of experiments we consider simultaneous atherosclerotic disease of vessels No. 9, 65, 66 with 50%, 50%, 50% lumens and with 50%, 30%, 30% lumens, respectively. The numerical results are qualitatively similar to those discussed above and thus are not presented here in detail. We notice the impact of the assumed atherosclerosis on the vessels No. 68 and No. 91: it is less pronounced than the impact of the single atherosclerotic vessel (the common carotid artery) with 30% lumen. We explain this fact by smoothing pressure and velocity profiles along the route in case of the simultaneous atherosclerotic disease.

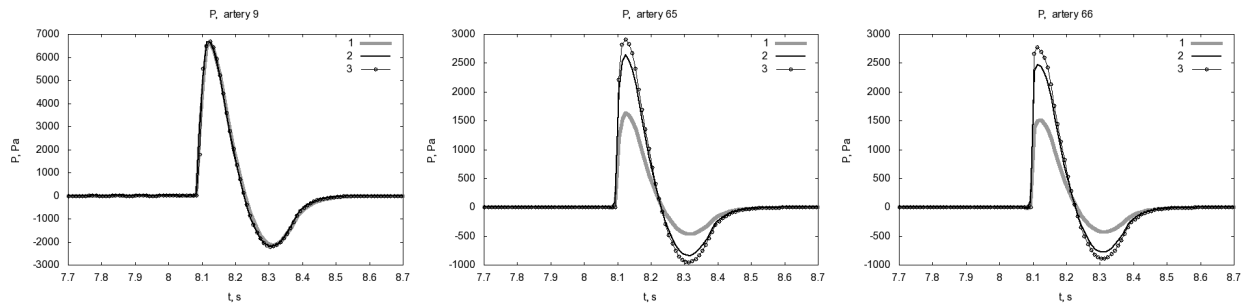


Figure 5: Pressure, Pa. 1 — 30% lumen, 2 — 50% lumen, 3 — healthy vessel.

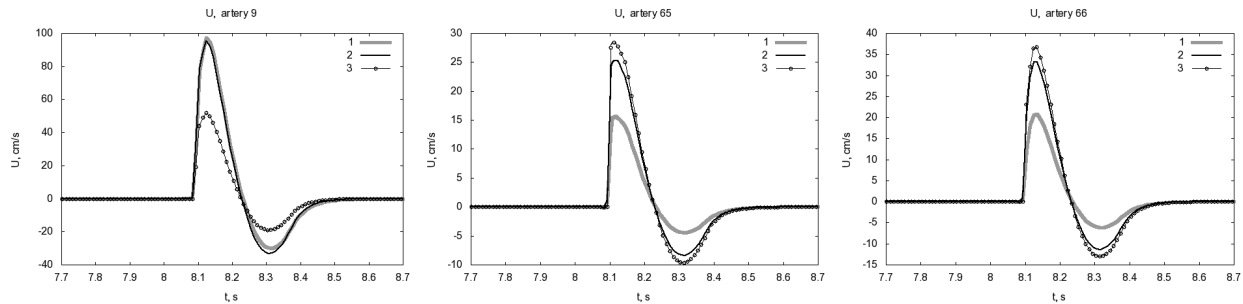


Figure 6: Velocity, cm/s. 1 — 30% lumen, 2 — 50% lumen, 3 — healthy vessel.

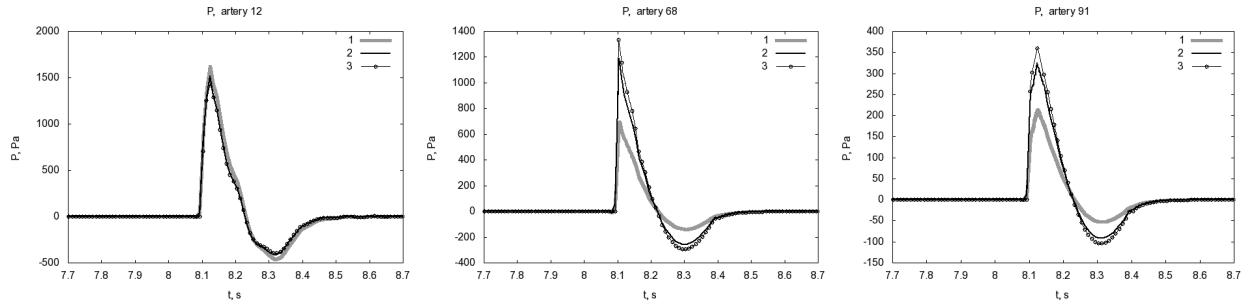


Figure 7: Pressure, Pa. 1 — 30% lumen, 2 — 50% lumen, 3 — healthy vessel.

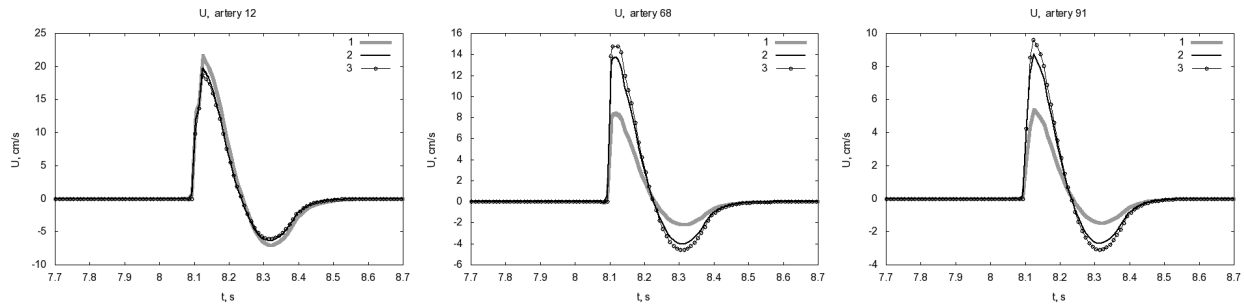


Figure 8: Velocity, cm/s. 1 — 30% lumen, 2 — 50% lumen, 3 — healthy vessel.

6. Conclusions

Most of the biological soft tissues demonstrate nonlinear strain-stress relationships, in particular, at high stresses. Elastic properties of atherosclerotic arteries can be represented by the three-layer composition of Neo-Hookean materials. In this paper we considered lengthy uniform atherosclerotic plaques in straight vessels and introduced the numerical fiber-spring model of atherosclerotic artery wall which accounts its three-layer Neo-Hookean structure. In our recent paper [17], we studied atherosclerotic artery wall as a composition of Hookean materials and showed that the numerical fiber-spring model could be applied to general shaped atherosclerotic plaques. In both papers, the elastic vessel wall numerical model produces the pressure to cross section relationship, or the wall state equation, which is the input function in the global network blood flow model [14]. The latter allows us to study the atherosclerotic disease impact on haemodynamics. Further development of this approach to the Neo-Hookean vessels and general shape vessels will be the subject of future investigations.

Acknowledgements

This work was partially supported by the Federal Program “Academic and pedagogical staff of innovative Russia”, RAS program “Basic Research for Medicine”, RFBR grants 08-01-00159, 09-01-00115, 10-01-91055, 11-01-00855.

References

- [1] G. Cheng, H. Loree, R. Kamm, M. Fishbein, R. Lee. *Distribution of circumferential stress in ruptured and stable atherosclerotic lesions: a structural analysis with histopathological correlation*. *Circulation*, 87 (1993), 1179–1187.
- [2] L. Formaggia, A. Quarteroni, A. Veneziani. *Cardiovascular mathematics*, Vol. 1. Heidelberg, Springer, 2009.
- [3] A. Green, J. Adkins. *Large Elastic Deformation*. Clarendon Press, Oxford, 1970.
- [4] G. Holzapfel, R. Ogden (Eds.). *Mechanics of Biological Tissue*, Vol. XII. 2006.
- [5] G. Holzapfel, R. Ogden. *Constitutive modelling of arteries*. *Proc. R. Soc. A*, 466 (2010), No. 2118, 1551–1597.
- [6] J. Humphrey. *Continuum biomechanics of soft biological tissues*. *Proc. R. Soc. Lond. A* 459, (2003), 3–46.
- [7] V. Koshelev, S. Mukhin, T. Sokolova, N. Sosnin, A. Favorski. *Mathematical modelling of cardio-vascular hemodynamics with account of neuroregulation*. *Matem. Mod.*, 19 (2007), No. 3, 15–28 (in Russian).
- [8] R. Lee, A. Grodzinsky, E. Frank, R. Kamm, F. Schoen. *Structure dependent dynamic mechanical behavior of fibrous caps from human atherosclerotic plaques*. *Circulation*, 83 (1991), 1764–1770.
- [9] J. Ohayon et al. *Influence of residual stress/strain on the biomechanical stability of vulnerable coronary plaques: Potential impact for evaluating the risk of plaque rupture*. *Am. J. Physiol. Heart Circ. Physiol.* 293 (2007), 1987–1996.
- [10] T.J. Pedley, X.Y. Luo. *Modelling flow and oscillations in collapsible tubes*. *Theor. Comp. Fluid Dyn.*, 10 (1998), No. 1–4, 277–294.
- [11] A. Quarteroni, L. Formaggia. *Mathematical modelling and numerical simulation of the cardiovascular system*. In: *Handbook of numerical analysis*, Vol. XII, Amsterdam, Elsevier, 2004, 3–127.
- [12] W. Riley, R. Barnes, et al. *Ultrasonic measurement of the elastic modulus of the common carotid. The Atherosclerosis Risk in Communities (ARIC) Study*. *Stroke*, 23 (1992), 952–956.
- [13] M. Rosar, C. Peskin. *Fluid flow in collapsible elastic tubes: a three-dimensional numerical model*. *New York J. Math.*, 7 (2001), 281–302.
- [14] S.S. Simakov, A.S. Kholodov. *Computational study of oxygen concentration in human blood under low frequency disturbances*. *Mat. Mod. Comp. Sim.*, 1 (2009), 283–295.

- [15] C. Tu, C. Peskin. *Stability and instability in the computation of flows with moving immersed boundaries: a comparison of three methods*. SIAM J. Sci. Stat. Comp., 6 (1992), No. 13, 1361–1376.
- [16] Y.V. Vassilevski, S.S. Simakov, S.A. Kapranov. *A multi-model approach to intravenous filter optimization*. Int. J. Num. Meth. Biomed. Engrg., 26 (2010), No. 7, 915–925.
- [17] Y. Vassilevski, S. Simakov, V. Salamatova, Y. Ivanov, T. Dobroserdova. *Blood flow simulation in atherosclerotic vascular network using fiber-spring representation of diseased wall*. Math. Model. Nat. Phen. (in press), 2011.
- [18] R. Vito, S. Dixon. *Blood vessel constitutive models, 1995-2002*. Annu. Rev. Biomed. Engrg., 5 (2003), 413–439.
- [19] R. Wulandana. *A nonlinear and inelastic constitutive equation for human cerebral arterial and aneurysm walls*. Dissertation, University of Pittsburgh, Pittsburgh, 2003.